Analysis of the Hessian for inverse scattering problems: II. Inverse medium scattering of acoustic waves



2012 Inverse Problems 28 055002

(http://iopscience.iop.org/0266-5611/28/5/055002)

IOP PUBLISHING INVERSE PROBLEMS

Inverse Problems **28** (2012) 055002 (17pp) doi:10.1088/0266-5611/28/5/055002

# Analysis of the Hessian for inverse scattering problems: II. Inverse medium scattering of acoustic waves

**Tan Bui-Thanh**[1] **and Omar Ghattas**[1,2,3]

[1] Institute for Computational Engineering and Sciences, The University of Texas at Austin, Austin, TX 78712, USA
[2] Jackson School of Geosciences, The University of Texas at Austin, Austin, TX 78712, USA
[3] Department of Mechanical Engineering, The University of Texas at Austin, Austin, TX 78712, USA

E-mail: tanbui@ices.utexas.edu and omar@ices.utexas.edu

Received 21 June 2011, in final form 29 February 2012
Published 4 April 2012
Online at stacks.iop.org/IP/28/055002

**Abstract**

We address the inverse problem for scattering of acoustic waves due to an inhomogeneous medium. We derive and analyze the Hessian in both Hölder and Sobolev spaces. Using an integral equation approach based on Newton potential theory and compact embeddings in Hölder and Sobolev spaces, we show that the Hessian can be decomposed into two components, both of which are shown to be compact operators. Numerical examples are presented to validate our theoretical results. The implication of the compactness of the Hessian is that for small data noise and model error, the discrete Hessian can be approximated by a low-rank matrix. This in turn enables fast solution of an appropriately regularized inverse problem, as well as Gaussian-based quantification of uncertainty in the estimated inhomogeneity.

(Some figures may appear in colour only in the online journal)

## 1. Introduction

A feature of many ill-posed inverse problems is that the Hessian operator of the data misfit functional is a compact operator with rapidly decaying eigenvalues. This is a manifestation of the typically sparse observations, which are informative about a limited number of modes of the infinite-dimensional field we seek to infer. The Hessian operator (and its finite-dimensional discretization) plays an important role in the analysis and solution of the inverse problem. In particular, the spectrum of the Hessian at the solution of the inverse problem determines the degree of ill-posedness and provides insight into the construction of appropriate regularization strategies. This has been observed, analyzed and exploited in several applications including shape optimization [1, 2] and inverse wave propagation [3–5], to name a few.

  

Moreover, the solution of the inverse problem by the gold standard iterative method—Newton's method—requires 'inversion' of the Hessian at each iteration. Compactness of the Hessian of the data misfit functional accompanied by sufficiently fast eigenvalue decay permits a low-rank approximation, which in turn facilitates rapid inversion or preconditioning of the regularized Hessian [3, 6]. Alternatively, the solution of the linear system arising at each Newton iteration by a conjugate gradient method can be very fast if the data misfit Hessian is compact with rapidly decaying eigenvalues and the conjugate gradient iteration is preconditioned by the regularization operator [7]. Finally, under a Gaussian approximation to the Bayesian solution of the inverse problem, the covariance of the posterior probability distribution is given by the inverse of the Hessian of the negative log-likelihood function. For Gaussian data noise and model error, this Hessian is given by an appropriately weighted Hessian of the data misfit operator, see, e.g., [8]. Here again, exploiting the low-rank character of the data misfit component of the Hessian is critical for rapidly approximating its inverse and hence the uncertainty in the inverse solution [4, 5, 9, 10].

In all of the cases described above, compactness of the data misfit Hessian is a critical feature that enables fast solution of the inverse problem, scalability of solvers to high dimensions and estimation of uncertainty in the solution. With this motivation, here, we analyze the Hessian operator for inverse medium acoustic scattering problems and study its compactness. Our analysis is based on an integral equation formulation of the Helmholtz equation, adjoint methods, and compact embeddings in Hölder and Sobolev spaces. These tools allow us to analyze the shape Hessian in detail.

The remainder of this paper is organized as follows. Section 2 briefly derives and formulates forward and inverse acoustic scattering problems due to bounded inhomogeneity. We then derive the Hessian for the inverse problem in section 3. Section 4 justifies the Hessian derivation by studying the well posedness of the (incremental) forward and (incremental) adjoint equations, and the regularity of their solutions. Next, we analyze the Hessian in Hölder spaces in section 5, and then, we extend the analysis to Sobolev spaces in section 6. In order to validate our theoretical developments, we provide numerical examples in section 7. Finally, the conclusions of this paper are presented in section 8.

## 2. Forward and inverse medium problems for acoustic scattering

In this section, we briefly discuss forward acoustic scattering problems due to bounded inhomogeneity and the corresponding inverse problems. Since both forward and inverse medium problems can be found elsewhere [11], our attention is to introduce necessary notations that will be used in our later derivations and analysis starting from section 3.

The scattering of time harmonic incident wave due to bounded inhomogeneity can be shown to be governed by the following Helmholtz equation [11]:

$$\nabla^2 U + k^2 n U = (1-n)k^2 U^{ic}, \quad \text{in } \mathbb{R}^d, \tag{1a}$$

$$\lim_{r\to\infty} r^{(d-1)/2}\left(\frac{\partial U}{\partial r} - ikU\right) = 0, \quad r = \|\mathbf{x}\|, \tag{1b}$$

where $U^{ic}$ is the incident wave that satisfies the Helmholtz equation $\nabla^2 U^{ic} + kU^{ic} = 0$, $k > 0$ is the wave number, $n > 0$ is the refractive index, which is assumed to be 1 for the free space, $d \in \{2, 3\}$ is the dimension of the background space, $i^2 = -1$, and $U$ is the scattered field. The radiation condition (1*b*) is assumed to be valid uniformly in all directions $\frac{\mathbf{x}}{\|\mathbf{x}\|}$, with $\mathbf{x}$ denoting the vector of spatial coordinates. In the rest of the paper, the inhomogeneity is assumed to be bounded, i.e. there exists some sufficiently large $a > 0$, such that $n(\mathbf{x}) = 1\ \forall \|\mathbf{x}\| > a$. In other words, $q = 1 - n$ has compact support in $\mathbb{R}^d$.

For the forward problem, $n$ is given and we solve the forward equations (1*a*) and (1*b*) for the scattered field $U$. For the inverse problem, on the other hand, given observation data $U^{\text{obs}}$ over some compact subset $\Omega^{\text{obs}} \subset \mathbb{R}^d$, we are asked to infer the distribution of the refractive index $n$. One way to solve the inverse problem is to cast it into the following PDE-constrained optimization problem:

$$\min_q \mathcal{J} = \int_{\mathbb{R}^d} K(\mathbf{x})|U - U^{\text{obs}}|^2 \,\mathrm{d}\Omega, \tag{2}$$

subject to the forward equations (1*a*) and (1*b*). Here, $K(\mathbf{x})$ denotes the observation operator whose support is $\Omega^{\text{obs}}$. In order to cover several interesting observation operators, $\Omega^{\text{obs}}$ is allowed to be quite general in this paper. In particular, it could be a closed subset in $\mathbb{R}^d$ or a relative closed subset of a manifold in $\mathbb{R}^d$. For example, in $\mathbb{R}^3$, $\Omega^{\text{obs}}$ could be a closed arc, or a closed curved, or a closed subset of a two-dimensional manifold, or some two-dimensional manifold. For convenience, we identify

$$\mathcal{K}\varphi = \int_{\mathbb{R}^d} K\varphi \,\mathrm{d}\Omega = \int_{\Omega^{obs}} \varphi\,(\mathbf{y})\ \mathrm{d}\mathbf{y}.$$

We also permit pointwise observation in our analysis, i.e. $\Omega^{\text{obs}} \equiv \{\mathbf{x}_j^{\text{obs}}\}_{j=1}^{N^{\text{obs}}}$, and in this case, we identify

$$\mathcal{K}\varphi = \int_{\mathbb{R}^d} K\varphi \,\mathrm{d}\Omega = \sum_{j=1}^{N^{\text{obs}}} \varphi\big(\mathbf{x}_j^{\text{obs}}\big). \tag{3}$$

## 3. Derivation of the Hessian

In this section, we derive the gradient and Hessian using a reduced space approach, and the justification for our derivations is provided in section 4. We begin with a useful observation on the radiation condition. Since the radiation condition (1*b*) is valid uniformly in all directions $\frac{\mathbf{x}}{\|\mathbf{x}\|}$, we rewrite the radiation condition as

$$\frac{\partial U}{\partial r} - ikU = \varphi(r) = o\big(r^{(1-d)/2}\big),$$

where $r$ is the radius of a sufficiently large circle $\Gamma_\infty$.

It can be seen that the cost functional (2) is real valued, while the constraints (1*a*)–(1*b*) are complex valued. Consequently, the usual Lagrangian approach will not make sense and care must be taken. Following Kreutz-Delgado [12], we define the Lagrangian as

$$\begin{aligned}\mathcal{L} = \mathcal{J} + \int_{\mathbb{R}^d} \overline{u}[\nabla^2 U + k^2 n U - k^2(1-n)U^{ic}]\,\mathrm{d}\Omega + \int_{\Gamma_\infty} \overline{u}_r \left(\frac{\partial U}{\partial r} - \mathrm{i}kU - \varphi\right) \mathrm{d}s \\ \times \int_{\mathbb{R}^d} u[\nabla^2 \overline{U} + k^2 n \overline{U} - k^2(1-n)\overline{U}^{ic}]\,\mathrm{d}\Omega + \int_{\Gamma_\infty} u_r \left(\frac{\partial \overline{U}}{\partial r} - \mathrm{i}k\overline{U} - \overline{\varphi}\right) \mathrm{d}s,\end{aligned}$$

where the overline, when acting on forward and adjoint states (and their variations), denotes the complex conjugate.

Taking the first variation of the Lagrangian with respect to $u$ and $u_r$ in the directions $\hat{u}$ and $\hat{u}_r$ and arguing that the variations $\hat{u}$ and $\hat{u}_r$ are arbitrary yield the forward equations (1*a*) and (1*b*).

Now taking the first variation of the Lagrangian with respect to $U$ in the direction $\hat{U}$ and arguing that the variation $\hat{U}$ is arbitrary yield the following adjoint equations:

$$\nabla^2 u + k^2 n u = -K(U - U^{\text{obs}}), \qquad \text{in } \mathbb{R}^d, \tag{4a}$$

$$\lim_{r\to\infty} r^{(d-1)/2}\left(\frac{\partial u}{\partial r} + \mathrm{i}ku\right) = 0, \qquad r = \|\mathbf{x}\|, \tag{4b}$$

and

$$u_r = -u \quad \text{on} \quad \Gamma_\infty.$$

If we eliminate $u_r$, the Lagrangian now becomes

$$\mathcal{L} = \mathcal{J} + \int_{\mathbb{R}^d} \overline{u}[\nabla^2 U + k^2 nU - k^2(1-n)U^{ic}]\,\mathrm{d}\Omega - \int_{\Gamma_\infty} \overline{u}\left(\frac{\partial U}{\partial r} - \mathrm{i}kU - \varphi\right)\mathrm{d}s$$
$$\times \int_{\mathbb{R}^d} u[\nabla^2 \overline{U} + k^2 n\overline{U} - k^2(1-n)\overline{U}^{ic}]\,\mathrm{d}\Omega - \int_{\Gamma_\infty} u\left(\frac{\partial \overline{U}}{\partial r} - \mathrm{i}k\overline{U} - \overline{\varphi}\right)\mathrm{d}s. \tag{5}$$

The gradient of the cost function acting in the direction $\hat{n}$ is simply the variation of the Lagrangian with respect to $q$ in the direction $\hat{n}$:

$$D\mathcal{J}(q;\hat{n}) = -k^2 \int_{\mathbb{R}^d} [\overline{u}(U + U^{ic}) + u(\overline{U} + \overline{U}^{ic})]\hat{n}\,\mathrm{d}\Omega. \tag{6}$$

For the sake of convenience in deriving the Hessian, the forward and adjoint equations are best expressed in the weak form. As a direct consequence of the above variational calculus steps, the forward equation in the weak form reads

$$\mathcal{S}(q,U) = \int_{\mathbb{R}^d} \overline{\hat{u}}[\nabla^2 U + k^2 nU - k^2(1-n)U^{ic}]\,\mathrm{d}\Omega - \int_{\Gamma_\infty} \overline{\hat{u}}\left(\frac{\partial U}{\partial r} - \mathrm{i}kU - \varphi\right)\mathrm{d}s = 0 \quad \forall \hat{u}. \tag{7}$$

Similarly, the adjoint equation in the weak form is given by

$$\mathcal{A}(q,U,u) = \int_{\mathbb{R}^d} \overline{\hat{U}}[\nabla^2 u + k^2 nu + K(U - U^{\mathrm{obs}})]\,\mathrm{d}\Omega - \int_{\Gamma_\infty} \overline{\hat{U}}\left(\frac{\partial u}{\partial r} + \mathrm{i}ku\right)\mathrm{d}s = 0 \quad \forall \hat{U}. \tag{8}$$

Next, the (reduced) Hessian acting in the directions $\hat{n}$ and $\tilde{n}$ is obtained by simply taking the first variation of the gradient $D\mathcal{J}(q,\hat{n})$ with respect to $q, U$ and $u$ in the directions $\tilde{n}, \tilde{U}$ and $\tilde{u}$:

$$D^2\mathcal{J}(q;\hat{n},\tilde{n}) = -k^2 \int_{\mathbb{R}^d} [\overline{\tilde{u}}(U + U^{ic}) + \tilde{u}(\overline{U} + \overline{U}^{ic}) + \overline{u}\tilde{U} + u\overline{\tilde{U}}]\hat{n}\,\mathrm{d}\Omega. \tag{9}$$

As mentioned at the beginning of this section, the reduced space approach is employed, and hence, the variations $\tilde{U}$ and $\tilde{u}$ cannot be arbitrary. In fact, they are only admissible if the forward and adjoint equations are satisfied. As a direct consequence, the first variations of $\mathcal{S}(q,U)$ and $\mathcal{A}(q,U,u)$ must vanish, i.e. $\tilde{U}$ is the solution of the following incremental forward equation:

$$\int_{\mathbb{R}^d} \overline{\hat{u}}[\nabla^2 \tilde{U} + k^2 n\tilde{U} - k^2\tilde{n}(U + U^{ic})]\,\mathrm{d}\Omega - \int_{\Gamma_\infty} \overline{\hat{u}}\left(\frac{\partial \tilde{U}}{\partial r} - \mathrm{i}k\tilde{U}\right)\mathrm{d}s = 0 \quad \forall \hat{u}, \tag{10}$$

and $\tilde{e}$ is the solution of the following incremental adjoint equation:

$$\int_{\mathbb{R}^d} \overline{\hat{U}}[\nabla^2 \tilde{u} + k^2 n\tilde{u} - k^2\tilde{n}u + K\tilde{U}]\,\mathrm{d}\Omega - \int_{\Gamma_\infty} \overline{\hat{U}}\left(\frac{\partial \tilde{u}}{\partial r} + ik\tilde{u}\right)\mathrm{d}s = 0 \quad \forall \hat{U}. \tag{11}$$

Consequently, the corresponding strong form of the incremental forward equation is

$$\nabla^2\tilde{U} + k^2 n\tilde{U} = k^2\tilde{n}(U + U^{ic}), \quad \text{in } \mathbb{R}^d, \tag{12a}$$

$$\lim_{r\to\infty} r^{(d-1)/2}\left(\frac{\partial \tilde{U}}{\partial r} - \mathrm{i}k\tilde{U}\right) = 0, \quad r = \|\mathbf{x}\|, \tag{12b}$$

and that of the incremental adjoint equation reads

$$\nabla^2\tilde{u} + k^2 n\tilde{u} = k^2\tilde{n}u - K\tilde{U}, \quad \text{in } \mathbb{R}^d, \tag{13a}$$

$$\lim_{r\to\infty} r^{(d-1)/2}\left(\frac{\partial\tilde{u}}{\partial r} + \mathrm{i}k\tilde{u}\right) = 0, \quad r = \|\mathbf{x}\|. \tag{13b}$$

Next, we need to convert the Hessian in (9) into a form that is convenient for our later analysis. The first step is to replace $\tilde{n}$ by $\hat{n}$ and choose $\hat{u} = \tilde{u}(\tilde{n})$ in the incremental forward equation (10). In the second step, we take $\hat{U} = \tilde{U}(\hat{n})$ in the incremental adjoint equation (11). The last step is to subtract the resulting incremental forward equation from the complex conjugate of the resulting incremental adjoint equation. After some simple integration by parts and cancellations, we obtain

$$\int_{\mathbb{R}^d} k^2\hat{n}\overline{\tilde{u}}(\tilde{n})(U + U^{ic})\,\mathrm{d}\Omega = \int_{\mathbb{R}^d} k^2\overline{u}\tilde{n}\tilde{U}(\hat{n})\,\mathrm{d}\Omega - \int_{\mathbb{R}^d} K\overline{\tilde{U}}(\tilde{n})\tilde{U}(\hat{n})\,\mathrm{d}\Omega. \tag{14}$$

Combining (9) and (14) gives the desired form of the Hessian as

$$D^2\mathcal{J}(q;\hat{n},\tilde{n}) = \underbrace{\int_{\mathbb{R}^d} K[\overline{\tilde{U}}(\tilde{n})\tilde{U}(\hat{n}) + \tilde{U}(\tilde{n})\overline{\tilde{U}}(\hat{n})]\,\mathrm{d}\Omega}_{\mathcal{H}_1(q;\hat{n},\tilde{n})}$$
$$- \underbrace{\left\{k^2\int_{\mathbb{R}^d}[\overline{u}\tilde{U}(\tilde{n}) + u\overline{\tilde{U}}(\tilde{n})]\hat{n}\,\mathrm{d}\Omega + k^2\int_{\mathbb{R}^d}[\overline{u}\tilde{U}(\hat{n}) + u\overline{\tilde{U}}(\hat{n})]\tilde{n}\,\mathrm{d}\Omega\right\}}_{\mathcal{H}_2(q;\hat{n},\tilde{n})}. \tag{15}$$

## 4. Regularity of the forward and adjoint solutions

In this section, we are going to justify what we have done in section 3 by studying the well posedness of the forward and adjoint equations and the regularity of their solutions. For sufficiently smooth inhomogeneity, the solutions turn out to be classical by using an integral equation method, as we shall show.

First, we introduce the following standard volume potentials (also known as Newton potentials) [13, 11]:

$$w(\mathbf{x}) = T\varphi(\mathbf{x}) = \int_{\mathbb{R}^N} \Phi(\mathbf{x},\mathbf{y})\varphi(\mathbf{y})\,\mathrm{d}\mathbf{y}, \quad \mathbf{x}\in\mathbb{R}^d, \tag{16}$$

where $\Phi$ is the fundamental solution of the (incremental) forward equation(s) defined as

$$\Phi(\mathbf{x},\mathbf{y}) = \begin{cases} \dfrac{\mathrm{i}}{4}H_0^1(\mathbf{x}-\mathbf{y}) & N=2 \\ \dfrac{\mathrm{e}^{\mathrm{i}k\|\mathbf{x}-\mathbf{y}\|}}{4\pi\,\|\mathbf{x}-\mathbf{y}\|} & N=3, \end{cases}$$

or the fundamental solution of the (incremental) adjoint solution(s):

$$\Phi(\mathbf{x},\mathbf{y}) = \begin{cases} -\dfrac{\mathrm{i}}{4}H_0^2(\mathbf{x}-\mathbf{y}) & N=2 \\ \dfrac{\mathrm{e}^{-\mathrm{i}k\|\mathbf{x}-\mathbf{y}\|}}{4\pi\,\|\mathbf{x}-\mathbf{y}\|} & N=3. \end{cases}$$

Next, we denote by $C^{m,\alpha}(\mathbb{R}^d)$ the space of $m$-times differentiable functions whose $m$th derivative is Hölder continuous with the exponent $\alpha$ in $\mathbb{R}^d$, and by $C_0^{m,\alpha}(\mathbb{R}^d)$ a subspace of $C^{m,\alpha}(\mathbb{R}^d)$ consisting of functions with compact support. The following mapping properties of the volume potential are important in what follows.

**Lemma 1.** *Let* $\varphi \in C_0(\mathbb{R}^d) \cap C^{m,\alpha}(\mathbb{R}^d)$, *where* $\alpha \in (0, 1]$ *and* $m \in \mathbb{N} \cup \{0\}$. *Then,* $w \in C^{m+2,\alpha}(\Omega)$, *and* $\|w\|_{C^{m+2,\alpha}(\Omega)} \leqslant c\,\|\varphi\|_{C^{m,\alpha}(\Omega)}$, *where* $\text{supp}\,(\varphi) \subset \Omega \subseteq \mathbb{R}^d$. *Furthermore, it holds that* $T$ *is compact in* $C^{p,\beta}(\Omega)$ *for* $m + \alpha \leqslant p + \beta \leqslant m + 2 + \alpha$.

**Proof.** We proceed by induction. The cases $m = 0, 1$ are proved and discussed in [13, 11]. Since differentiation and integration can be interchanged [13, 11], the partial derivative in the $x_j$ direction reads

$$\begin{aligned} D_{x_j} w(\mathbf{x}) &= \int_{\mathbb{R}^d} \varphi(\mathbf{y}) D_{x_j} \Phi(\mathbf{x}, \mathbf{y})\, \mathrm{d}\Omega = -\int_{\Omega} \varphi(\mathbf{y}) D_{y_j} \Phi(\mathbf{x}, \mathbf{y})\, \mathrm{d}\mathbf{y} \\ &= -\underbrace{\int_{\partial\Omega} \Phi(\mathbf{x}, \mathbf{y})\, \varphi(\mathbf{y}) n_j\, \mathrm{d}s}_{0} + \int_{\Omega} \Phi(\mathbf{x}, \mathbf{y})\, D_{y_j} \varphi(\mathbf{y})\, \mathrm{d}\mathbf{y}, \end{aligned} \tag{17}$$

where $n_j$ denotes the $j$th component of the normal vector of $\partial\Omega$, and we have used the fact that $D_{x_j}\Phi(\mathbf{x}, \mathbf{y}) = -D_{y_j}\Phi(\mathbf{x}, \mathbf{y})$ and $\varphi(\mathbf{y}) = 0$ on $\partial\Omega$. Since $D_{y_j}\varphi(\mathbf{y}) \in C_0(\mathbb{R}^d) \cap C^{m-1,\alpha}(\mathbb{R}^d)$, we conclude, by the induction hypothesis, that $D_{x_j} w(\mathbf{x}) \in C^{m+1,\alpha}(\Omega)$. This implies $w(\mathbf{x}) \in C^{m+2,\alpha}(\Omega)$.

The second assertion is readily proved by the induction hypothesis

$$\left\|D_{x_j} w\right\|_{C^{m+1,\alpha}(\Omega)} \leqslant C \left\|D_{x_j}\varphi\right\|_{C^{m-1,\alpha}(\Omega)}$$

and the definition of Hölder norms [14, 11]. The third assertion is trivial due to the compact embeddings in Hölder spaces [14]. □

In order to use lemma 1 and the Riesz–Fredholm theory [15, 16] to study the well posedness of the forward and adjoint equations, we first recall the following Green formula [11] for $u \in C^2(\Omega) \cap C(\overline{\Omega})$ :

$$u(\mathbf{x}) = \int_{\partial\Omega} \left[\Phi \frac{\partial u}{\partial \mathbf{n}} - u \frac{\partial \Phi}{\partial \mathbf{y}}\right] \mathrm{d}s - \int_{\Omega} \Phi(\nabla^2 u + k^2 u)\, \mathrm{d}\Omega,$$

where $\mathbf{n}$ denotes the unit outward normal vector of $\partial\Omega$. Denote

$$\mathcal{T}[q]\varphi(\mathbf{x}) = k^2 \int_{\Omega} \Phi(\mathbf{x}, \mathbf{y}) q(\mathbf{y}) \varphi(\mathbf{y})\, \mathrm{d}\mathbf{y}, \quad \mathbf{x} \in \Omega,$$

and $I$ as the identity operator. We now have the following integral representations for the forward and the adjoint equations.

**Theorem 1.** *Let* $\Omega \subseteq \mathbb{R}^d$, *and* $q, \tilde{n} \in C_0^{m,\alpha}(\Omega)$, *where* $\alpha \in (0, 1]$ *and* $m \in \mathbb{N} \cup \{0\}$. *In addition, let* $p$ *and* $\beta$ *satisfy* $m + \alpha \leqslant p + \beta \leqslant m + 2 + \alpha$. *The forward, incremental forward, adjoint and incremental adjoint equations are well posed in the sense that they are equivalent to the following Lippmann–Schwinger-type integral equations.*

*(i) The forward integral equation*

$$(I + \mathcal{T}[q])U(\mathbf{x}) = -\mathcal{T}[q]U^{ic}(\mathbf{x}) \tag{18}$$

*has a unique solution* $U$ *in* $C^{p,\beta}(\Omega)$ *and the solution depends continuously on the data.*

*(ii) The incremental forward integral equation*

$$(I + \mathcal{T}[q])\tilde{U}(\mathbf{x}) = \mathcal{T}[\tilde{n}](U + U^{ic})(\mathbf{x}) \tag{19}$$

*has a unique solution* $\tilde{U}$ *in* $C^{p,\beta}(\Omega)$ *and the solution depends continuously on the data.*

*(iii) The adjoint integral equation*

$$(I + \mathcal{T}[q])u(\mathbf{x}) = \int_{\Omega^{obs}} \Phi(\mathbf{x}, \mathbf{y}) K(U - U^{\text{obs}})(\mathbf{y})\, \mathrm{d}\mathbf{y} \tag{20}$$

*has a unique solution in* $C^{m,\alpha}(\Omega)$ *and the solution depends continuously on the data.*

*(iv) The incremental adjoint integral equation*

$$(I + \mathcal{T}[q])\,\tilde{u}(\mathbf{x}) = \mathcal{T}[\tilde{n}]u(\mathbf{x}) + \int_{\Omega^{obs}} \Phi(\mathbf{x}, \mathbf{y}) K\tilde{U}(\mathbf{y})\,\mathrm{d}\mathbf{y} \tag{21}$$

*has a unique solution in $C^{m,\alpha}(\Omega)$ and the solution depends continuously on the data.*

**Proof.** The equivalence for the forward equation can be found in [11, 17] for the case $q \in C_0^1(\mathbb{R}^3)$. The generalization to the case $q \in C_0^{m,\alpha}(\Omega)$ is straightforward. By the same token, we have the equivalence for other equations. This suggests that we need to study only the well posedness of the integral equations.

By lemma 1, $\mathcal{T}$ is compact in $C^{p,\beta}(\Omega)$, and $\mathcal{T}[q]U^{ic}(\mathbf{x}) \in C^{p,\beta}(\Omega)$ due to the analyticity of the incident wave $U^{ic}$. The Riesz–Fredholm theory [15] therefore applies, and the forward integral equation has a unique solution in $C^{p,\beta}(\Omega)$. Moreover, $(I + \mathcal{T}[q])^{-1}$ is bounded, i.e. the solution depends continuously on $\mathcal{T}[q]U^{ic}(\mathbf{x})$ in the $C^{p,\beta}$-norm. The proof for incremental forward solution (19) follows the same line by observing that the right-hand side of (19) belongs to $C^{p,\beta}(\Omega)$ from lemma 1.

As for the adjoint equation, owing to $\Omega^{\text{obs}} \cap \text{supp}(q) = \emptyset$ and the analyticity of $\Phi(\mathbf{x}, \mathbf{y})$, the right-hand side of (20) is certainly a function in $C^{p,\beta}(\Omega)$ (in fact it is analytic in $\mathbb{R}^d \setminus \text{supp}(\Omega^{\text{obs}})$), and again the Riesz–Fredholm theory gives the desired results. Finally, for the incremental adjoint integral equation, observe that the first term on the right-hand side of (21) belongs to $C^{p,\beta}(\Omega)$ and the second term is analytic on $\Omega$. As a result, the right-hand side of equation (21) is a function in $C^{p,\beta}(\Omega)$. The conclusions are now readily verified by the Riesz–Fredholm theory. □

We are now in the position to justify our derivations of gradient and Hessian in section 3.

**Theorem 2.** *Let $\Omega \subset \mathbb{R}^d$ be a bounded domain. Assume that $q$, $\hat{n}$ and $\tilde{n}$ belong to $C_0^\alpha(\Omega)$. Then, the cost functional (2) is twice continuously Fréchet differentiable, and hence, the gradient (6) and Hessian (15) are well defined.*

**Proof.** First, observe that we have used Gâteaux derivatives to derive the gradient and Hessian in section 3. Now it is evident that both $D\mathcal{J}(q; \hat{n})$ and $D^2\mathcal{J}(q; \hat{n}, \tilde{n})$ are linear and continuous with respect to $\hat{n}$ (and $\tilde{n}$) since $U$, $u$, $\tilde{U}$ and $\tilde{u}$ belong to $C^{2,\alpha}(\Omega)$ by theorem 1. Moreover, continuous dependence on $q$ of $U$ from theorem 1 implies the continuous dependence on $q$ of $u$, $\tilde{U}$ and $\tilde{u}$, which in turn implies the continuity of $D\mathcal{J}(q; \hat{n})$ and $D^2\mathcal{J}(q; \hat{n}, \tilde{n})$ with respect to $q$. Hence, a classical result on sufficiency for the Fréchet derivative [18] ends the proof. □

## 5. Analysis of the Hessian in Hölder spaces

In this section, we study the behavior of the Hessian at a fixed refractive distribution $n$, i.e. $q = 1 - n \in C_0^{m,\alpha}(\Omega)$. Unlike the shape Hessian that is only compact at the optimal solution as we have analyzed in the first part of this work [19], the Hessian of the inverse medium scattering problem turns out to be compact for all $q$ as we shall show. For concreteness, we restricted ourselves to two exemplary cases of the observation operator, namely the observation is everywhere on a compact subset $\Omega^{\text{obs}}$ having non-trivial $r$-dimensional Lesbegue measure for some $1 \leqslant r \leqslant d$ (we call this case as continuous observation) and pointwise observation $\Omega^{\text{obs}} = \{\mathbf{x}_j^{\text{obs}}\}_{j=1}^{N^{\text{obs}}}$.

From theorem 1, observe that the incremental forward solution $\tilde{U}$ can be identified as the following operator composition:

$$\tilde{U} : C_0^{m,\alpha}(\Omega) \ni \tilde{n} \mapsto \tilde{U}(\tilde{n}) = (I + \mathcal{T}[q])^{-1}\mathcal{T}[\tilde{n}](U + U^{ic}) \in C^{p,\beta}(\Omega),$$

which is compact since it is the composition of the continuous operator $(I + \mathcal{T}[q])^{-1}$ (owing to the Riesz–Fredholm theory) and the compact operator $\mathcal{T}[\tilde{n}]\left(U + U^{ic}\right)$ (due to lemma 1). As a result, $\tilde{U}(\tilde{n})\Big|_{\Omega^{\text{obs}}}$ is still a compact operator since restricting to $\Omega^{\text{obs}}$ is a continuous operation.

If the observation is continuous, the Gauss–Newton part of the Hessian, namely $\mathcal{H}_1(n; \hat{n}, \tilde{n})$, can now be rewritten as

$$\mathcal{H}_1(q; \hat{n}, \tilde{n}) = 2\mathscr{R}(\tilde{U}(\hat{n}), \tilde{U}(\tilde{n}))_{L^2(\Omega)^{\text{obs}}} = 2\mathscr{R}(\tilde{U}^*\tilde{U}(\hat{n}), \tilde{n})_{L^2(\Omega)^{\text{obs}}},$$

where the real operator $\mathscr{R}$ extracts the real part of its argument and $(\cdot)^*$ denotes the adjoint operator. In this form, $\mathcal{H}_1(n)$ is evidently compact due to the compactness of $\tilde{U}(\hat{n})|_{\Omega^{\text{obs}}}$.

If, on the other hand, the observation is pointwise, then the evaluation of $\tilde{U}(\tilde{n})$ at $\mathbf{x}_j^{\text{obs}}$ can be written as

$$\begin{aligned}\tilde{U}(\tilde{n})(\mathbf{x}_j^{\text{obs}}) &= (-k^2 q\Phi_j, \tilde{U}(\tilde{n}))_{L^2(\Omega)} + (k^2\tilde{n}\Phi_j, U + U^{ic})_{L^2(\Omega)} \\ &= (k^2\Phi_j(U + U^{ic}) - \tilde{U}^*(k^2 q\Phi_j), \tilde{n})_{L^2(\Omega)} \\ &= (\Psi_j, \tilde{n})_{L^2(\Omega)},\end{aligned}$$

where $\Phi_j = \Phi(\mathbf{x}_j^{\text{obs}}, \mathbf{y})$ and $\Psi_j = k^2\Phi_j(U+U^{ic}) - \tilde{U}^*(k^2 q\Phi_j)$. In this case, the Gauss–Newton part $\mathcal{H}_1(n; \hat{n}, \tilde{n})$ reads

$$\mathcal{H}_1(q; \hat{n}, \tilde{n}) = 2\mathscr{R}\left(\left(\sum_j^{N^{\text{obs}}} \overline{\Psi}_j\Psi_j, \tilde{n}\right)_{L^2(\Omega)}, \hat{n}\right)_{L^2(\Omega)},$$

which shows that the dimension of the range of $\mathcal{H}_1(q)$ is at most $N^{\text{obs}}$. Consequently, $\mathcal{H}_1(q)$ is a compact operator. We summarize the above result on the compactness of $\mathcal{H}_1(q)$ in the following theorem, which is valid for both continuous and pointwise observation cases.

**Theorem 3.** *$\mathcal{H}_1(q)$, as a continuous bilinear form on $C_0^{m,\alpha}(\mathbb{R}^d) \times C_0^{m,\alpha}(\mathbb{R}^d)$, is a compact operator.*

The analysis of $\mathcal{H}_2(q)$ is somewhat easier as we shall now show.

**Theorem 4.** *$\mathcal{H}_2(q)$, as a continuous bilinear form on $C_0^{m,\alpha}(\mathbb{R}^d) \times C_0^{m,\alpha}(\mathbb{R}^d)$, is a compact operator.*

**Proof.** Rewrite $\mathcal{H}_2(q; \tilde{n}, \hat{n})$ as

$$\mathcal{H}_2(q; \tilde{n}; \hat{n}) = 2k^2\mathscr{R}\int_\Omega [\overline{u}\tilde{U}(\hat{n})\tilde{n} + \overline{u}\tilde{U}(\tilde{n})\hat{n}]\,\mathrm{d}\Omega = 2k^2\mathscr{R}(\tilde{U}^*(\overline{u}\tilde{n}) + \overline{u}\tilde{U}(\tilde{n}), \hat{n})_{L^2(\Omega)}.$$

We conclude that $\mathcal{H}_2(q)$ is compact by the following three observations. First, the incremental forward solution $\tilde{U}$ can be identified as a compact operator in $C_0^{m,\alpha}(\Omega)$ as discussed above. Second, multiplication by $\overline{u} \in C_0^{m,\alpha}(\Omega)$ is a continuous operation (see, e.g., [19]). Third, the sum of two compact operators is again compact. □

We close this section by observing that the full Hessian is the difference of two compact operators, and it is therefore compact as well.

## 6. Analysis of the Hessian in Sobolev spaces

Similar to the first part of our work [19], we shall extend the analysis in Hölder spaces to Sobolev spaces. A result similar to that of lemma 1 is now stated.

**Lemma 2.** *Assume that $\varphi$ is bounded and integrable, $\Omega \subset \mathbb{R}^d$ is a bounded domain and* $\text{supp}(\varphi) \subset \Omega$. *Then, $T$ defined in (16) maps $H^m(\Omega)$ continuously to $H^{m+2}(\Omega)$ for $m \in \mathbb{N} \cup \{0\}$.*

**Proof.** We proceed by induction. The case $m = 0$ has already been proved in [11]. Now assume that the assertion holds for $m-1$, and we need to show that it also holds for $m$. Since boundedness and integrability of $\varphi$ enable integration and differentiation interchange [20], (17) holds. By the induction hypothesis, $D_{x_j} w(\mathbf{x}) \in H^{m+1}(\Omega)$, and this implies $w(\mathbf{x}) = T\varphi(\mathbf{x}) \in H^{m+2}(\Omega)$. □

By compact embeddings in Sobolev spaces [21, 22], one can see that $T$ is compact in $H^s(\Omega)$ for $m \leqslant s \leqslant m+2$. This fact is used to prove the following compactness of the Hessian in Sobolev spaces.

**Theorem 5.** *Let $q$ be bounded, integrable, and $q \in H^m(\Omega)$, where $\Omega$ is a bounded domain, and* $\text{supp}(q) \subset \Omega \subset \mathbb{R}^d$. *Then, the Hessian, $\mathcal{H}(q) = \mathcal{H}_1(q) - \mathcal{H}_2(q)$, is a compact operator in $H^m(\Omega)$.*

**Proof.** The proof follows the same line as in section 5 by using lemma 2, and hence omitted. □

## 7. Numerical results

In this section, we numerically compute the eigenvalues of the shape Hessian (9) to validate our theoretical developments in sections 5 and 6. For the purpose of demonstration, it is sufficient to consider two-dimensional problems for which we can use an efficient coupled finite-element and boundary integral equation approach. The detailed description of our coupling strategy is now presented.

### *7.1. Forward scattering problem*

We decompose the forward problem into two sub-problems, namely, the interior sub-problem given by

$$\nabla^2 U^{\text{in}} + k^2 n U^{\text{in}} = (1-n)k^2 U^{ic}, \quad \text{in } \Omega, \tag{22a}$$

$$\frac{\partial U^{\text{in}}}{\partial \mathbf{n}} + \mathrm{i}k U^{\text{in}} = \psi, \quad \text{on } \partial\Omega, \tag{22b}$$

and the exterior sub-problem given by

$$\nabla^2 U^{\text{ex}} + k^2 n U^{\text{ex}} = 0, \quad \text{in } \mathbb{R}^d \setminus \overline{\Omega}, \tag{23a}$$

$$\frac{\partial U^{\text{ex}}}{\partial \mathbf{n}} + \mathrm{i}k U^{\text{ex}} = \psi, \quad \text{on } \partial\Omega, \tag{23b}$$

$$\lim_{r\to\infty} r^{(d-1)/2} \left( \frac{\partial U^{\text{ex}}}{\partial r} - \mathrm{i}k U^{\text{ex}} \right) = 0, \tag{23c}$$

where $\psi$ is the unknown coupling function. It is easy to show that the weak formulation of the interior problem (22) reads

$$\int_\Omega \nabla U^{\text{in}} \cdot \nabla v \, \mathrm{d}\Omega - k^2 \int_\Omega n U^{\text{in}} v \, \mathrm{d}\Omega + \mathrm{i}k \int_{\partial\Omega} U^{\text{in}} v \, \mathrm{d}s = \mathrm{i}k \int_{\partial\Omega} \psi v \, \mathrm{d}s - k^2 \int_\Omega q U^{ic} v \, \mathrm{d}\Omega \tag{24}$$

and that the boundary integral equation formulation of the exterior problem (23) reads

$$(I - D - \mathrm{i}kS)U^{\text{ex}} = -S\psi, \tag{25}$$

with the representation

$$U^{\text{ex}}(\mathbf{x}) = \int_{\partial\Omega} U^{\text{ex}}(\mathbf{y}) \left[ \frac{\partial \Phi(\mathbf{x}, \mathbf{y})}{\partial \mathbf{n}} + ik\Phi(\mathbf{x}, \mathbf{y}) \right] \mathrm{d}s(\mathbf{y}) - \int_{\partial\Omega} \Phi(\mathbf{x}, \mathbf{y}) \, \psi(\mathbf{y}) \, \mathrm{d}s(\mathbf{y}),$$

and with $S$ and $D$ as the following standard surface single- and double-layer potentials [11]:

$$S\varphi(\mathbf{x}) = 2 \int_{\partial\Omega} \Phi(\mathbf{x}, \mathbf{y}) \varphi(\mathbf{y}) \, \mathrm{d}s(\mathbf{y}), \quad \mathbf{x} \in \partial\Omega,$$

$$D\varphi(\mathbf{x}) = 2 \int_{\partial\Omega} \frac{\partial \Phi(\mathbf{x}, \mathbf{y})}{\partial \mathbf{n}(\mathbf{y})} \varphi(\mathbf{y}) \, \mathrm{d}s(\mathbf{y}), \quad \mathbf{x} \in \partial\Omega.$$

The interior and exterior solutions are matched by satisfying the following continuity condition at the interface $\partial\Omega$:

$$U^{\text{in}} = U^{\text{ex}}, \quad \text{on } \partial\Omega, \tag{26}$$

which, together with (22) and (23), implies the continuity in the normal derivative:

$$\frac{\partial U^{\text{in}}}{\partial \mathbf{n}} = \frac{\partial U^{\text{ex}}}{\partial \mathbf{n}}, \quad \text{on } \partial\Omega.$$

Inspired by the coupling approach in [23], we choose to use the finite-element method (FEM) for solving the interior problem (24), while we solve the exterior boundary integral equation (25) using the Nyström method [11, 19]. Now, the nature of the coupling is implicit, i.e. in order to solve for $U^{\text{in}}$ and $U^{\text{ex}}$, the availability of $\psi$ is required. On the other hand, in order to solve (26) for $\psi$, one has to supply $U^{\text{in}}$ and $U^{\text{ex}}$. Moreover, matching the finite-element and Nyström methods may not be trivial since the finite-element solution is defined variationally, while the Nyström solution is pointwise in nature. We adopt a simple decoupling approach due to Kirsch and Monk [23] in which $\psi$ is represented by trigonometric polynomials of order $M$:

$$\psi = \sum_{j=-M}^{M-1} \alpha_j \phi_j, \quad \phi_j = \mathrm{e}^{\mathrm{i}jt}, \quad t \in [0, 2\pi].$$

With this representation, one can solve the interior and exterior problems independently for each basis function $\varphi_j$. Then, the unknown coefficients $\alpha_j$ can be solved for by employing a Galerkin projection on (26):

$$\int_{\partial\Omega} (U^{\text{in}} - U^{\text{ex}}) \overline{\phi}_j \, \mathrm{d}s = 0, \quad j = -M, \ldots, M-1,$$

where $\overline{\phi}_j$ denotes the complex conjugate of $\phi_j$.

In this paper, we use the Nyström quadrature for all line integrals along $\partial\Omega$. This implies that one has to interpolate the FEM solution at the Nyström points. To avoid this extra interpolation problem, we generate the FEM mesh such that all the mesh vertices on $\partial\Omega$ coincide with the Nyström points. We therefore simply read off the FEM nodal solutions for the Nyström quadrature.

Since the coupled finite-element and boundary integral approach—together with its discretization—for the adjoint, incremental forward, incremental adjoint problems is similar, we will present only the sub-problems and the continuity condition at the interface in the next three subsections.

*7.2. Adjoint scattering problem*

Similar to the forward scattering problem, the interior sub-problem for the adjoint equation reads

$$\nabla^2 u^{\text{in}} + k^2 n u^{\text{in}} = 0, \quad \text{in } \Omega,$$
$$\frac{\partial u^{\text{in}}}{\partial \mathbf{n}} + \mathrm{i}k u^{\text{in}} = \psi, \quad \text{on } \partial\Omega,$$

while the exterior problem reads

$$\nabla^2 u^{\text{ex}} + k^2 n u^{\text{ex}} = -K(U - U^{\text{obs}}), \quad \text{in } \mathbb{R}^d \setminus \overline{\Omega},$$
$$\frac{\partial u^{\text{ex}}}{\partial \mathbf{n}} + \mathrm{i}k u^{\text{ex}} = \psi, \quad \text{on } \partial\Omega,$$
$$\lim_{r\to\infty} r^{(d-1)/2}\left(\frac{\partial u^{\text{ex}}}{\partial r} + \mathrm{i}k u^{\text{ex}}\right) = 0.$$

The interior and exterior solutions are matched by satisfying the following continuity condition at the interface $\partial\Omega$:

$$u^{\text{in}} = u^{\text{ex}}, \quad \text{on } \partial\Omega,$$

*7.3. Incremental forward scattering problem*

For the incremental forward problem, we choose the interior sub-problem as

$$\nabla^2 \tilde{U}^{\text{in}} + k^2 n \tilde{U}^{\text{in}} = -\tilde{n}k^2(U + U^{ic}), \quad \text{in } \Omega,$$
$$\frac{\partial \tilde{U}^{\text{in}}}{\partial \mathbf{n}} + \mathrm{i}k \tilde{U}^{\text{in}} = \psi, \quad \text{on } \partial\Omega,$$

and the exterior sub-problem as

$$\nabla^2 \tilde{U}^{\text{ex}} + k^2 n \tilde{U}^{\text{ex}} = 0, \quad \text{in } \mathbb{R}^d \setminus \overline{\Omega},$$
$$\frac{\partial \tilde{U}^{\text{ex}}}{\partial \mathbf{n}} + \mathrm{i}k \tilde{U}^{\text{ex}} = \psi, \quad \text{on } \partial\Omega,$$
$$\lim_{r\to\infty} r^{(d-1)/2}\left(\frac{\partial \tilde{U}^{\text{ex}}}{\partial r} - \mathrm{i}k \tilde{U}^{\text{ex}}\right) = 0.$$

The interior and exterior solutions are matched by satisfying the following continuity condition at the interface $\partial\Omega$:

$$\tilde{U}^{\text{in}} = \tilde{U}^{\text{ex}}, \quad \text{on } \partial\Omega.$$

*7.4. Incremental adjoint scattering problem*

Similar to the adjoint scattering problem, the interior sub-problem reads

$$\nabla^2 \tilde{u}^{\text{in}} + k^2 n \tilde{u}^{\text{in}} = -\tilde{n}k^2 u, \quad \text{in } \Omega,$$
$$\frac{\partial \tilde{u}^{\text{in}}}{\partial \mathbf{n}} + \mathrm{i}k \tilde{u}^{\text{in}} = \psi, \quad \text{on } \partial\Omega,$$

while the exterior problem reads

$$\nabla^2 \tilde{u}^{\text{ex}} + k^2 n \tilde{u}^{\text{ex}} = -K\tilde{U}, \quad \text{in } \mathbb{R}^d \setminus \overline{\Omega},$$
$$\frac{\partial \tilde{u}^{\text{ex}}}{\partial \mathbf{n}} + \mathrm{i}k \tilde{u}^{\text{ex}} = \psi, \quad \text{on } \partial\Omega,$$
$$\lim_{r\to\infty} r^{(d-1)/2}\left(\frac{\partial \tilde{u}^{\text{ex}}}{\partial r} + \mathrm{i}k \tilde{u}^{\text{ex}}\right) = 0.$$

The interior and exterior solutions are matched by satisfying the following continuity condition at the interface $\partial\Omega$:

$$\tilde{u}^{\text{in}} = \tilde{u}^{\text{ex}}, \quad \text{on } \partial\Omega,$$

For numerical results, a second-order FEM on an unstructured triangular mesh is used for the interior sub-problem, and a Nyström method with 240 equally distributed (in $t$) points is used for the exterior sub-problem. The wave number is chosen to be $k = 10$, while the number of trigonometric polynomials is 60 by taking $M = 30$. For brevity, only results for pointwise observation are presented since those for continuous observation are similar. The observational data $U^{\text{obs}}$ is synthesized at $N^{\text{obs}} = 31$ points equally distributed in the interval $y \in [-10, 10]$ and at $x = b = -10$, unless otherwise stated. For the sake of convenience, the following simple inhomogeneity [23] is used:

$$n(r) = \begin{cases} 1 + c(1 - r^4)^2 & r \leqslant 1 \\ 1 & r \geqslant 1, \end{cases} \qquad r = \|\mathbf{x}\|, \tag{27}$$

where $c$ is some scalar constant, in particular, we choose $c = 0.5$ for the synthesization. As a result, we can choose $\Omega$ as the unit circle. Finally, the incident wave is assumed to be of the form $U^{ic} = \mathrm{e}^{\mathrm{i}kx}$. Our goal is to numerically show that the Hessian is compact for any bounded inhomogeneity $n$. However, for convenience, we choose $n$ of the form (27), and in particular, we choose to study the discrete Hessian at various values of $c$. Numerically, we are able to examine the necessary condition for the Hessian operator to be compact (and hence the ill-posedness of the inverse problem), namely the convergence to zero of the Hessian eigenvalues. However, even in this case, it is impossible to study all the eigenvalues since they are countably infinite. We will therefore resort to investigating a small dominant part of the spectrum, from which we draw conclusions. In the rest of this section, we 'measure' the degree of ill-posedness by the magnitude of eigenvalues. For example, given two ill-posed inverse problems, i.e. the Hessian eigenvalues decay to zero, we say one problem is more ill-posed than another if the eigenvalues of the former are smaller than those of the latter at the same indices.

A second-order triangular mesh with 2738 elements and 5597 nodes is generated, which permits us to represent the refractive index as

$$n = \sum_{m=1}^{5597} n_m \xi_m,$$

where $\xi_m$ are the nodal finite-element basis functions. The continuous optimization variable $n$ has been cast into 5597 discrete nodal unknowns $n_m$, and hence, the Hessian is a $5597 \times 5597$ matrix. The real and imaginary parts of the forward and adjoint solutions at $c = 1$ are shown in figure 1.

Away from the optimal solution, i.e. at $c = 0.5$, the Hessian may not be (semi-) positive definite, and for this reason, we will present only the eigenvalue magnitudes. Figure 2 shows the first 1000 eigenvalues that are largest in magnitudes for $c = \{1, 0.4, 0.499, 0.5\}$. As can be seen, the eigenvalues decay exponentially at the optimal inhomogeneity, but the decay rate is rather slow otherwise. Moreover, closer to the optimal inhomogeneity, the eigenvalue is smaller for a same index, indicating the increasing ill-posedness of the inverse problem as the optimal solution is approached. Note that at the optimal solution, the full Hessian collapses to the Gauss–Newton part, i.e. $\mathcal{H}_1$, since $\mathcal{H}_2 = 0$.

Next, we keep $c = 1$ fixed, but allow the wave number $k$ to change. Figure 3 shows the first 1000 eigenvalues that are largest in magnitudes for $k = \{10, 5, 1, 0.1\}$. It can be observed that as the wave number decreases, so do the Hessian eigenvalues. This is expected since

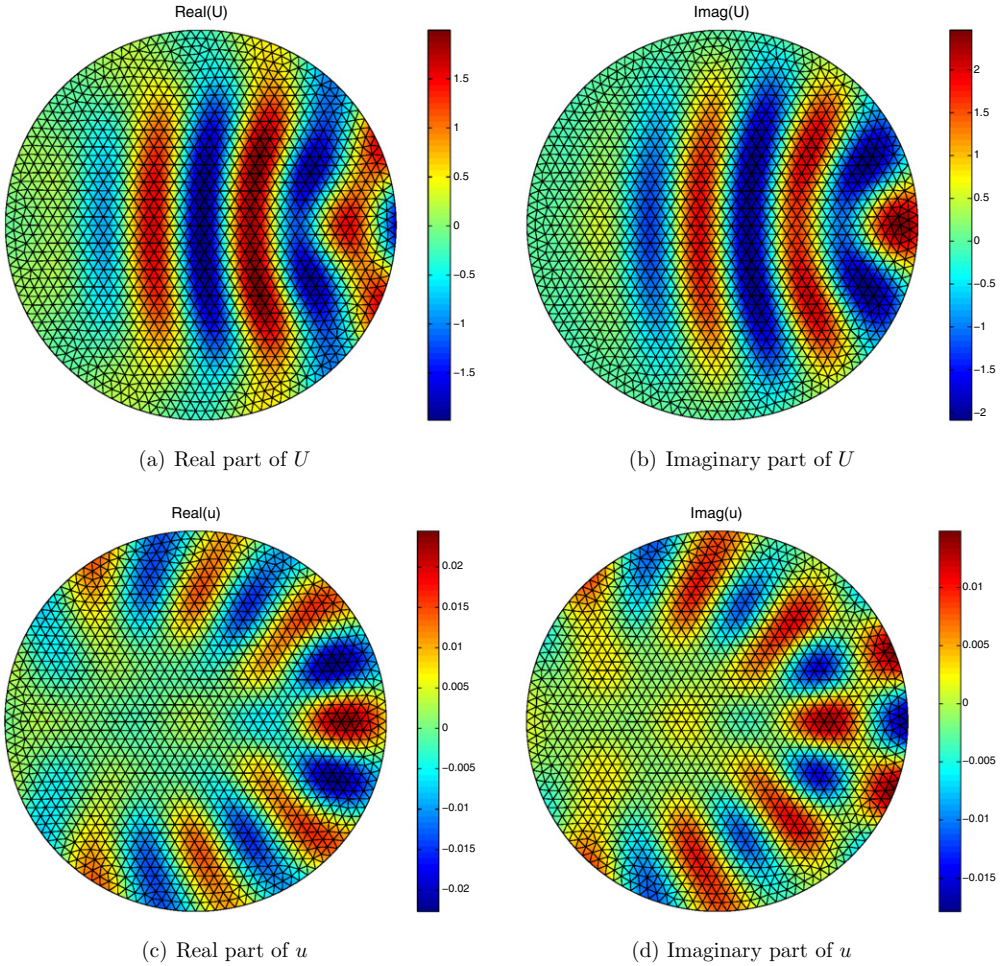


(a) Real part of $U$ (b) Imaginary part of $U$

(c) Real part of $u$ (d) Imaginary part of $u$

**Figure 1.** Real and imaginary parts of the forward and adjoint solutions for $n$ given in (27) with $c = 1$.

intuitively the larger the wave number, the easier the detection of the inhomogeneity, and hence, the problem is less ill-posed. As can also be seen, the asymptotic decay rate seems to be similar for all cases.

We now keep $c = 1$ and $k = 10$ fixed, but let the observation radius $b$ vary. We present in figure 4 the first 1000 eigenvalues that are largest in magnitudes for $b = \{1, 10, 100, 10\,000\}$. As the observations are taken further away from the inhomogeneity region, the Hessian eigenvalues are smaller. Again, for all cases, the eigenvalues decay to zero, indicating the compactness of the Hessian operator. The result suggests that observations should be carried out as close as possible to the inhomogeneity for the inverse problem to be less ill-posed.

In order to study the affect of observations on the ill-posedness of the inverse problem, we fix $c = 1$, $k = 10$ and $b = -10$, and let $N^{\text{obs}}$ points be equally distributed in the interval $y \in [-100, 100]$. Figure 5 shows the first 1000 eigenvalues that are largest in magnitudes for $N^{\text{obs}} = \{1, 51, 101, 1001\}$. One can observe that as more observation points are added, the inverse problem is less ill-posed since the eigenvalues increase. That is, as more information

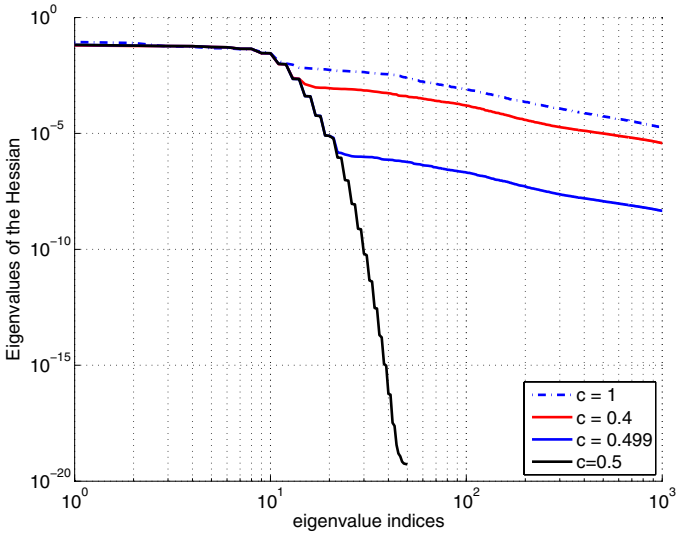


**Figure 2.** Magnitudes of the first 1000 eigenvalues of the Hessian at $n$ ($c = \{1, 0.4, 0.499, 0.5\}$) given in (27).

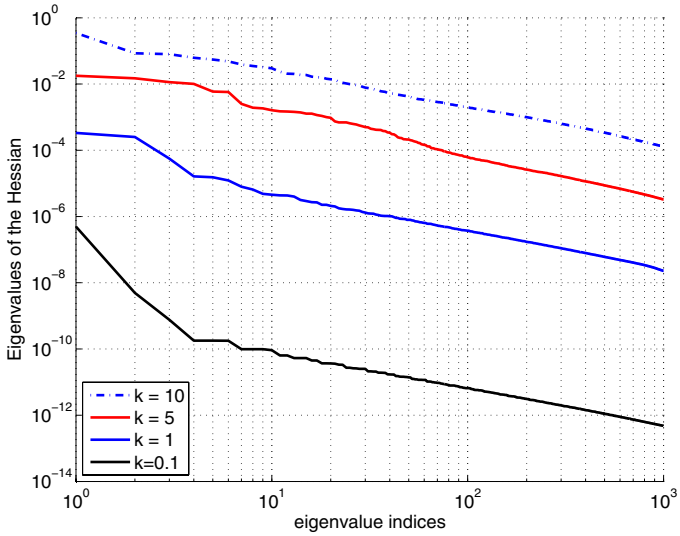


**Figure 3.** Magnitudes of the first 1000 eigenvalues of the Hessian for $k = \{10, 5, 1, 0.1\}$.

about the inhomogeneity is available, the problem of reconstructing it is more well posed, agreeing with our assumption.

Finally, we study the dependence on mesh refinement of the Gauss–Newton Hessian dominant spectrum. Figure 6 shows the first 100 dominant eigenvalues for three different mesh sizes $h = \{0.1, 0.05, 0.025\}$. As can be observed, the dominant part of the spectrum is numerically independent of the mesh size. This result is consistent with the numerical results

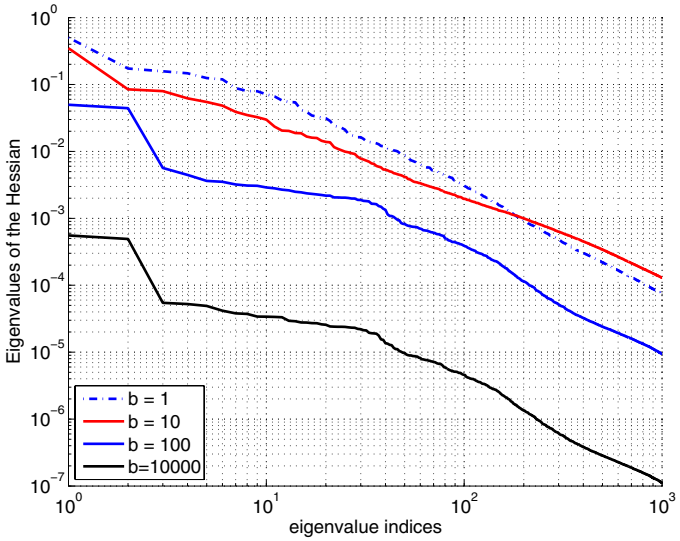


**Figure 4.** Magnitudes of the first 1000 eigenvalues of the Hessian for $b = \{1, 10, 100, 10\,000\}$.

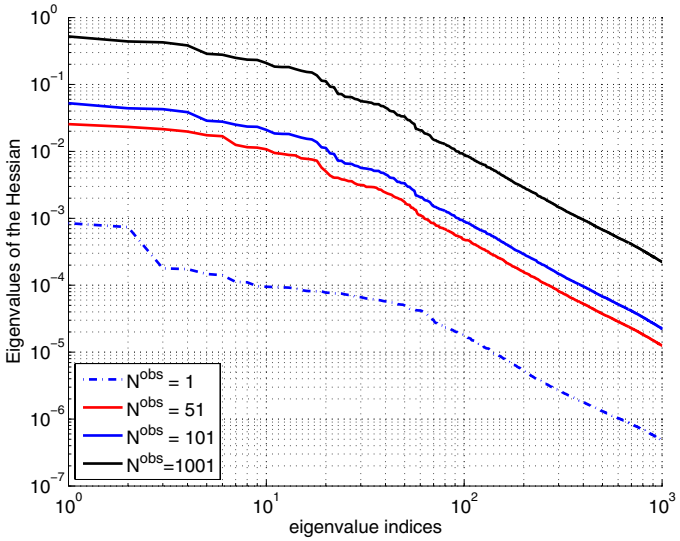


**Figure 5.** Magnitudes of the first 1000 eigenvalues of the Hessian for $N^{\text{obs}} = \{1, 51, 101, 1001\}$.

in the first part of our work [19] in which we numerically show that the Gauss–Newton Hessian dominant spectrum is independent of the mesh size regardless of the shape.

## 8. Conclusions

We have analyzed the Hessian stemming from the inverse problem of scattering of acoustic waves due to bounded inhomogeneity. Unlike our companion paper on inverse shape scattering

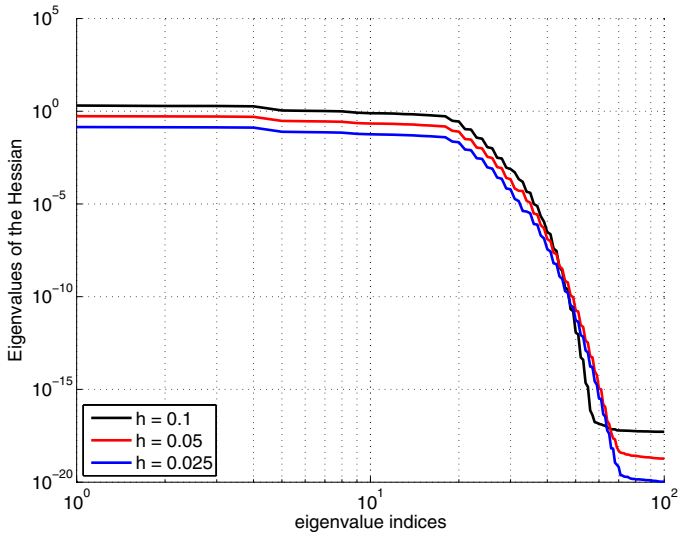


**Figure 6.** The first 100 dominant eigenvalues of the Hessian for $h = \{0.1, 0.05, 0.025\}$ with $c = 0.5$.

problems [19] for which only the Gauss–Newton Hessian is compact, the full Hessian operator has been shown to be compact for inverse medium scattering problems. Our analysis starts with a study on the smoothness of the scattering solution based on the Newton potential theory and the Riesz–Fredholm framework. Then, together with compact embeddings in Hölder and Sobolev spaces, we are able to prove the compactness of the Hessian operator in both Hölder- and Sobolev-space settings, and for both two and three dimensions. Our theoretical results have been validated numerically in several scenarios. Our future work also includes application of the Hessian knowledge and the decaying eigenvalues in constructing effective algorithms for inverse medium scattering of acoustic waves.

## Acknowledgments

This research was supported by AFOSR grant FA9550-09-1-0608; DOE grants DE-SC0002710, DE-FG02-08ER25860, DE-FC52-08NA28615 and DEFC02-06ER25782; and NSF grants CMS-1028889, OPP-0941678, DMS-0724746 and CMS-0619078. The authors would like to thank the anonymous referees for their useful comments and suggestions.

## References

[1] Eppler K and Harbrecht H 2008 Compact gradient tracking in shape optimization *Comput. Optim. Appl.* **39** 297–318

[2] Eppler K and Harbrecht H 2006 Coupling of FEM-BEM in shape optimization *Numer. Math.* **104** 47–68

[3] Demanet L, Ltourneau P-D, Boumal N, Calandra H, Chiu J and Snelson S 2011 Matrix probing: a randomized preconditioner for the wave-equation Hessian arXiv:1101.3615v1 [math.NA]

[4] Flath H P, Wilcox L C, Akçelik V, Hill J, van Bloemen Waanders B and Ghattas O 2011 Fast algorithms for Bayesian uncertainty quantification in large-scale linear inverse problems based on low-rank partial Hessian approximations *SIAM J. Sci. Comput.* **33** 407–32

[5] Bui-Thanh T, Burstedde C, Ghattas O, Martin J, Stadler G and Wilcox L C 2012 Scalable parallel algorithms for uncertainty quantification in high dimensional inverse problems (in preparation)

[6] Chaillat S and Biros G 2012 FaIMS: a fast algorithm for the inverse medium problem with multiple frequencies and multiple sources for the scalar Helmholtz equations (under review)
[7] Björk A 1996 *Numerical Methods for Least Squares Problems* (Philadelphia, PA: SIAM)
[8] Tarantola A 2005 *Inverse Problem Theory and Methods for Model Parameter Estimation* (Philadelphia, PA: SIAM)
[9] Martin J, Wilcox L C, Burstedde C and Ghattas O 2012 A stochastic Newton MCMC method for large scale statistical inverse problems with application to seismic inversion *SIAM J. Sci. Comput.* at press
[10] Bui-Thanh T, Ghattas O and Higdon D 2012 Adaptive Hessian-based non-stationary Gaussian process response surface method for probability density approximation with application to Bayesian solution of large-scale inverse problems (submitted)
[11] Colton D and Kress R 1998 *Inverse Acoustic and Electromagnetic Scattering* (*Applied Mathematical Sciences* vol 93) 2nd edn (Berlin: Springer)
[12] Kreutz-Delgado K 2009 The complex gradient operator and the CR-calculus *Technical Report UCSD-ECE275CG-S2009v1.0* University of California, San Diego, CA
[13] Gilbarg D and Trudinger N S 2001 *Elliptic Partial Differential Equations of Second Order (Classics in Mathematics)* 2nd edn (Berlin: Springer)
[14] Zeidler E 1986 *Nonlinear Functional Analysis and Its Applications: I. Fixed Point Theorems* (Berlin: Springer)
[15] Colton D and Kress R 1983 *Integral Equation Methods in Scattering Theory* (New York: Wiley)
[16] Kress R 1989 *Linear Integral Equations* (Berlin: Springer)
[17] Kirsch A 1996 *An Introduction to the Mathematical Theory of Inverse Problems* (Berlin: Springer)
[18] Blanchard P and Brüning E 2003 *Mathematical Methods in Physics* (Basel: Birkhäuser)
[19] Bui-Thanh T and Ghattas O 2012 Analysis of the Hessian for inverse scattering problems: I. Inverse shape scattering of acoustic waves *Inverse Problems* **28** 055001
[20] Helms Lester L 2009 *Potential Theory* (Berlin: Springer)
[21] Arbogast T and Bona J L 2008 *Methods of Applied Mathematics (Lecture Notes in Applied Mathematics)* (Austin, TX: University of Texas)
[22] McLean W 2000 *Strongly Elliptic Systems and Boundary Integral Equations* (Cambridge: Cambridge University Press)
[23] Kirsch A and Monk P 1994 An analysis of the coupling of finite-element and Nyström methods in acoustic scattering *IMA J Numer. Anal.* **14** 523–44